Gas Phase Structure of Micro-Hydrated $[Mn(ClO_4)]^+$ and $[Mn_2(ClO_4)_3]^+$ Ions Probed by Infrared Spectroscopy

Rajeev K. Sinha, Edith Nicol,* Vincent Steinmetz, and Philippe Maître
Laboratoire de Chimie Physique, UMR8000 CNRS, Université Paris Sud 11, Orsay, France

Gas-phase infrared photodissociation spectroscopy is reported for the microsolvated $[Mn(ClO_4)(H_2O)_n]^+$ and $[Mn_2(ClO_4)_3(H_2O)_n]^+$ complexes from $n = 2$ to 5. Electrosprayed ions are isolated in an ion-trap where they are photodissociated. The 2600–3800 cm^{-1} spectral region associated with the OH stretching mode is scanned with a relatively low-power infrared table-top laser, which is used in combination with a CO_2 laser to enhance the photofragmentation yield of these strongly bound ions. Hydrogen bonding is evidenced by a relatively broad band red-shifted from the free OH region. Band assignment based on quantum chemical calculations suggest that there is formation of water–perchlorate hydrogen bond within the first coordination shell of high-spin Mn(II). Although the observed spectral features are also compatible with the formation of structures with double-acceptor water in the second shell, these structures are found relatively high in energy compared with structures with all water directly bound to manganese. Using the highly intense IR beam of the free electron laser CLIO in the 800–1700 cm^{-1}, we were also able to characterize the coordination mode (η^2) of perchlorate for two clusters. The comparison of experimental and calculated spectra suggests that the perchlorate Cl–O stretches are unexpectedly underestimated at the B3LYP level, while they are correctly described at the MP2 level allowing for spectral assignment. (J Am Soc Mass Spectrom 2010, 21, 758–772) © 2010 Published by Elsevier Inc. on behalf of American Society for Mass Spectrometry

The solvation of metal cations is of utmost importance for understanding many chemical and biological processes [1, 2]. Insights into the hydration of ions in condensed phase can be obtained by investigating models systems in the gas-phase [3, 4], and gas-phase water metal ion complexes have been the subject of recent reviews [5–7].

Gas-phase infrared photodissociation spectroscopy can provide useful structural information on water solvated metal ions [8–10]. As in the case of protonated water clusters [11], the frequencies of the water OH stretches can shift substantially with water–water hydrogen bond formation, and information about ion–water interaction and metal coordination number can be derived. Water solvated alkali [10, 12–15] and alkaline earth [16–21] metals, as well as various transition-metals [17, 22–30] have been studied. IR spectroscopy in the OH stretching region is usually carried out with a relatively low intensity table-top laser. The principal limitation of this method is that the cation-water binding energy must be less than the IR photon energy. This is not often realized, but as the water cluster size increases, the water binding energy decreases, so that the IR induced photodissociation can be monitored [18, 19, 22, 26]. For smaller size and more strongly bound water solvated metal cluster ions, a rare gas "tag" can be employed [23, 24, 28, 29]. Alternatively, highly intense IR free electron lasers offer a complementary IR spectral range (100–2000 cm^{-1}) [31, 32], which can provide information on the coordination mode of ligands bound to transition-metal cations [33–38].

Water solvation of $[Mn(ClO_4)]^+$ and $[Mn_2(ClO_4)_3]^+$ is studied here using a combination of gas-phase infrared spectroscopy and quantum chemical methods. While studies of water solvated clusters of singly or multiply charged metal ions have been the subject of numerous investigations, solvation of gas-phase ion-pairs has received less attention [39]. IR spectra of $[Mn(ClO_4)(H_2O)_{2-5}]^+$ and $[Mn_2(ClO_4)_3(H_2O)_{2-5}]^+$ cluster ions have been recorded in OH stretching region, and we here present our first results obtained for relatively strongly bound ions using a combination of an optical parametric oscillator/amplifier (OPO/OPA) with a CO_2 laser. While these spectra provide interesting information on the hydrogen bond formation as a function of the cluster size, the coordination mode of the perchlorate has also been probed by recording IR spectra in the 800–1700 cm^{-1} energy range. Infrared spectra are calculated for various

Address reprint requests to Dr. P. Maître, Laboratoire de Chimie Physique, Université Paris-Sud 11 UMR8000 CNRS, Faculté des sciences, bâtiment 350, 91405 Orsay cedex, France. E-mail: philippe.maitre@u-psud.fr

* Present address: Laboratoire des Mécanismes Reactionnels, Département de Chimie, Ecole Polytechnique, CNRS UMR7651, 91128 Palaiseau Cedex, France.

1044-0305/10/$32.00
doi:10.1016/j.jasms.2010.02.014

Published online February 11, 2010
Received January 31, 2010
Revised February 8, 2010
Accepted February 8, 2010

structure associated with different bonding motifs, allowing for band assignment of the main infrared features observed in both spectral ranges.

Experimental and Theoretical Methods

Experimental

Infrared (IR) spectroscopy of gas-phase $[Mn(ClO_4)(H_2O)_{2-5}]^+$ and $[Mn_2(ClO_4)_3(H_2O)_{2-5}]^+$ cluster ions is performed employing two experimental setups based on the coupling of an ion trap with two IR lasers.

For the IR spectroscopy of selected $[Mn(ClO_4)(H_2O)_{2-5}]^+$ and $[Mn_2(ClO_4)_3(H_2O)_{2-5}]^+$ cluster ions in the 1000–2000 c^{-1} spectral range, an experimental setup consisting of a quadrupole ion trap (Bruker Esquire 3000+) coupled with the Infrared Free Electron Lasers (IR FEL) from the Centre Laser Infrarouge d'Orsay (CLIO) was used [40]. IR-FELs have been shown to be particularly well suited for performing IRMPD spectroscopy of strongly bound ions in the so-called infrared fingerprint range, i.e., between 800 and 2500 cm^{-1} [31, 32]. The high intensity together with the pulse structure of these lasers both contribute to the efficient energy pumping of the molecular ions through a multiple photon absorption process [31].

An optical parametric oscillator/amplifier (OPO/OPA from LaserVision, Bellevue, WA, USA) laser system was used for recording the IR spectra in the OH stretching region. This laser system is pumped by an Innolas Spitlight 600 (München, Germany) non-seeded Nd:YAG (1064 nm, 550 mJ/pulse, bandwidth ~1 cm^{-1}) laser running at 25 Hz and delivering pulses of 4–6 ns duration. Typical output energy of the OPO/OPA was 12–13 mJ/pulse at 3600 cm^{-1} with a 3–4 cm^{-1} (FWHM) bandwidth. IR spectra in the 2600–3800 cm^{-1} spectral range of the clusters ions were recorded using a 7 tesla Fourier Transform Ion Cyclotron Resonance (FT-ICR) tandem mass spectrometer coupled with this OPO/OPA laser system [41–43].

For some of the cluster ions studied here, it was found that the output energy of the OPO/OPA system was not sufficient for inducing their fragmentation. As we will see in the next section, IR spectra could be recorded with OPO/OPA in association with a 10 W continuous wave (CW) broadband CO_2 laser. It should be noted that combination of tunable IR laser with line tunable CO_2 laser has been used earlier [44, 45].

In the present case, a broadband CO_2 laser (BFI Optilas, Evry, France) was used in a pulse mode. With the OPO/OPA tuned on a vibrational transition of a cluster ion, a significant enhancement of the fragmentation signal could be observed by irradiating the ions using a few ms long CO_2 pulse following each OPO/OPA pulse, the delay being about ~1 μs. Using this configuration, one can expect that multiple CO_2 photons can be absorbed following the absorption of one (or few) photon(s) delivered by the OPO/OPA laser system. Considering the complex motion of the ions and the large size of the ion cloud in the ICR cell, the spatial overlap of the two IR beams is very critical. The superposition of the two laser beams along the magnetic field of the ICR cell is achieved using a spherical mirror with a 3 mm diameter hole. While this focusing mirror is used for steering the OPO/OPA beam towards the ICR cell, the CO_2 laser beam steered from a flat gold coated mirror goes through the hole. The CO_2 pulse length and spatial overlap of the two lasers were optimized by monitoring the fragmentation yield when the OPO/OPA laser is tuned on a vibrational resonance of the ion of interest.

Hydrated manganese salt ions are prepared in an electrospray ionization (ESI) source using a 10^{-5} M solution of $Mn(ClO_4)_2.6H_2O$ hydrated salt in purified water. The solution is introduced in the source using direct infusion with a syringe pump with a flow rate of 3 μL/min. Spray voltage of 4000 V and capillary temperature of 120 °C are used. Mass-selected cluster ions are thermalized through multiple collisions with helium buffer gas in the quadrupole ion trap. Using the hydrid FT-ICR (Bruker Apex Qe), following their mass-selection, ions can also be collisionally thermalized in a hexapole ion trap under argon pressure (~10^{-3} mbar) before transferring them to the ICR cell. Comparison of the IRMPD bandwidth obtained using these two tandem mass spectrometers when performing IR spectroscopy with the IR FEL suggests that comparable thermalization of the mass-selected ions can be achieved using the two setups [41].

Theoretical

Quantum chemical calculations were carried out on the $[Mn(ClO_4)(H_2O)_{2-5}]^+$ and $[Mn_2(ClO_4)_3(H_2O)_{2-5}]^+$ cluster ions to elucidate their vibrational band assignments. On the basis of previously reported studies of water solvated metal ions, one can anticipate the different bonding motifs characterizing the arrangement of the water molecules at play for the low-energy structures. The characterization of the stationary points on the potential energy surface (PES) of these cluster ions was performed using the B3LYP hybrid density functional theory (DFT) approach. In all cases, only the high-spin state has been considered for the present Mn(II) containing clusters where the metal is bound to low-field ligands. Following a first exploration of the PES using the 6-31G* basis set, the lowest energy structures associated with each bonding motif were subsequently characterized using a triple zeta valence basis set supplemented with diffuse functions on the heavy atoms and polarization functions on all atoms (6-311+G(d,p)).

In the case of metal aqua ions, it has recently been shown that ab initio molecular orbital methods provide a more balanced treatment of metal-ligand and hydrogen bond strengths than DFT based approaches resulting in low coordination numbers for the metal [46]. In the particular case of metal aqua Mn^{2+} system, Stace and coworkers have recently shown that satisfactory

results could be obtained at the MP2 level [47]. For instance, in the case of $[Mn(H_2O)_6]^{2+}$ ion, while the lowest energy structure at the DFT (BP86 using a TZP basis set) level is characterized by a coordination number (CN) of four for Mn^{2+} [48], the correct energy ordering is obtained using the MP2 approach which predicts hexacoordinated Mn^{2+} structures to be lower in energy [47]. In the case of the monometallic $[Mn(ClO_4)(H_2O)_n]^+$ (n = 2–5) clusters, single point MP2/6-311+G(d,p) calculations were carried out using the B3LYP/6-311+G(d,p) geometries. Furthermore, in the case of $[Mn(ClO_4)(H_2O)_3]^+$, five structures characterized by different bonding schemes were fully characterized at the MP2/6-311+G(d,p) level.

Harmonic vibrational frequencies are determined, thus ensuring that the stationary points correspond to minima on the potential surface. For comparison with experimental infrared spectra in the OH stretching region, all the computed vibrational frequencies were scaled by a factor of 0.96. Spectral assignment in the 1000–2000 cm^{-1} was more difficult, and a detailed comparison of experimental and both MP2 and B3LYP theoretical spectra is proposed in the case of $[Mn(ClO_4)(H_2O)_3]^+$. All the calculations reported here are performed with Gaussian 03 suite of program [49].

Results and Discussion

Enhanced Fragmentation Efficiency Using CO_2 Laser

Upon energy activation of the cluster ions, loss of water molecules is expected as evidenced by collision induced dissociation (CID) of mass selected $[Mn(ClO_4)(H_2O)_{2-5}]^+$ or $[Mn_2(ClO_4)_3(H_2O)_{2-5}]^+$ cluster ions. As can be seen in Figure 1a, upon collisional activation with argon, sequential loss of one and two water molecules from $[Mn(ClO_4)(H_2O)_3]^+$ is observed. In the IRMPD spectra recorded under the present experimental conditions, loss of one water molecule is observed as the most favorable channel of fragmentation. On the other hand, loss of a second water molecule is observed but with much lesser extent compared with that of the CID spectrum.

As emphasized in the method section, combination of two lasers had to be used to achieve an efficient fragmentation of some clusters, and this was especially critical for $[Mn(ClO_4)(H_2O)_2]^+$ and $[Mn_2(ClO_4)_3(H_2O)_2]^+$. As found in the case of water solvated Ca^{2+} dications [18], as well as for transition-metal cations and dications [22], the metal-water binding energy is large for low-coordination numbers, leading to an inefficient photodissociation signal [18]. On the other hand, photoevaporation of water molecules can be achieved for larger size clusters. In the present case, it is therefore not surprising that the combination of the two lasers was required in the case of $[Mn(ClO_4)(H_2O)_2]^+$. It should be noted, however, that this combination turned out to be also useful for large size clusters, e.g., $[Mn(ClO_4)(H_2O)_5]^+$.

The advantage of using this combination of the two lasers is illustrated using the case of $[Mn(ClO_4)(H_2O)_2]^+$. Three IR induced fragmentation spectra are provided in parts b–d of Figure 1. When the OPO/OPA is tuned on resonance at 3600 cm^{-1} (Figure 1b), loss of one water from $[Mn(ClO_4)(H_2O)_2]^+$ can be observed, but the signal/noise ratio is low. However, when the CO_2 laser is used in conjunction with the OPO/OPA tuned at 3600 cm^{-1} (Figure 1c), the fragmentation yield increases by a factor of five. This was achieved by increasing the pulse length of the CO_2 laser up to 18 ms for the $[Mn_2(ClO_4)_3(H_2O)_2]^+$ cluster ion. As illustrated in Figure 1d, it should be emphasized that IR spectra were recorded in background free conditions since no fragmentation was observed when the OPO/OPA laser was tuned off resonance (3450 cm^{-1}).

Overview of IR Spectra in the OH Stretching Region

Gas-phase IR spectra of $[Mn(ClO_4)(H_2O)_{2-5}]^+$ and $[Mn_2(ClO_4)_3(H_2O)_{2-5}]^+$ cluster ions are shown in Figure 2a and b, respectively). All spectra were recorded in the 3200–3800 cm^{-1} energy range, and the 2800–3200 cm^{-1} range was also explored for the $[Mn(ClO_4)(H_2O)_3]^+$, $[Mn(ClO_4)(H_2O)_5]^+$, and $[Mn_2(ClO_4)_3(H_2O)_4]^+$ complexes. In all cases, only water loss was observed. In the case of the $[Mn(ClO_4)(H_2O)_{2-5}]^+$ clusters, only two IR features could be clearly observed. They are found in the high-frequency range (3600–3800 cm^{-1}) of the spectrum in regions labeled A and B in Figure 2a. In the cases of the $[Mn_2(ClO_4)_3(H_2O)_4]^+$ and $[Mn_2(ClO_4)_3(H_2O)_5]^+$ bimetallic clusters, however, besides the features in regions A and B of the spectrum, one can clearly observe a third feature at ~3500 cm^{-1} (labeled C in Figure 2b), which is much broader than features in regions A and B. On the basis of recent gas-phase IR spectroscopic investigations of water solvated metal cations, a first interpretation of these features can be made.

Coordination of water to a metal cation induces a red-shift of the symmetric and asymmetric OH stretches with respect to their positions (3649 and 3731 cm^{-1}, respectively) [50] for the free water molecule. This has been evidenced for numerous metal hydrated systems [23, 51], and also for protonated water clusters [11, 44]. This red-shift can be understood [11] as resulting from a partial electron-transfer from the water molecule to the metal cation. These free OH stretches have been found in the 3600–3800 cm^{-1} energy range. For all the $[Mn(ClO_4)(H_2O)_{2-5}]^+$ and $[Mn_2(ClO_4)_3(H_2O)_{2-5}]^+$ ionic clusters ions studied here, the bands observed in regions A and B (Figure 2) can thus be safely assigned to the ν_{sym} and ν_{asym} modes of vibration of water molecule coordinated to the metal ion.

Upon addition of several water molecules and approaching the maximum coordination number of the metal, competition between direct coordination to the metal cation and formation of water–water hydrogen

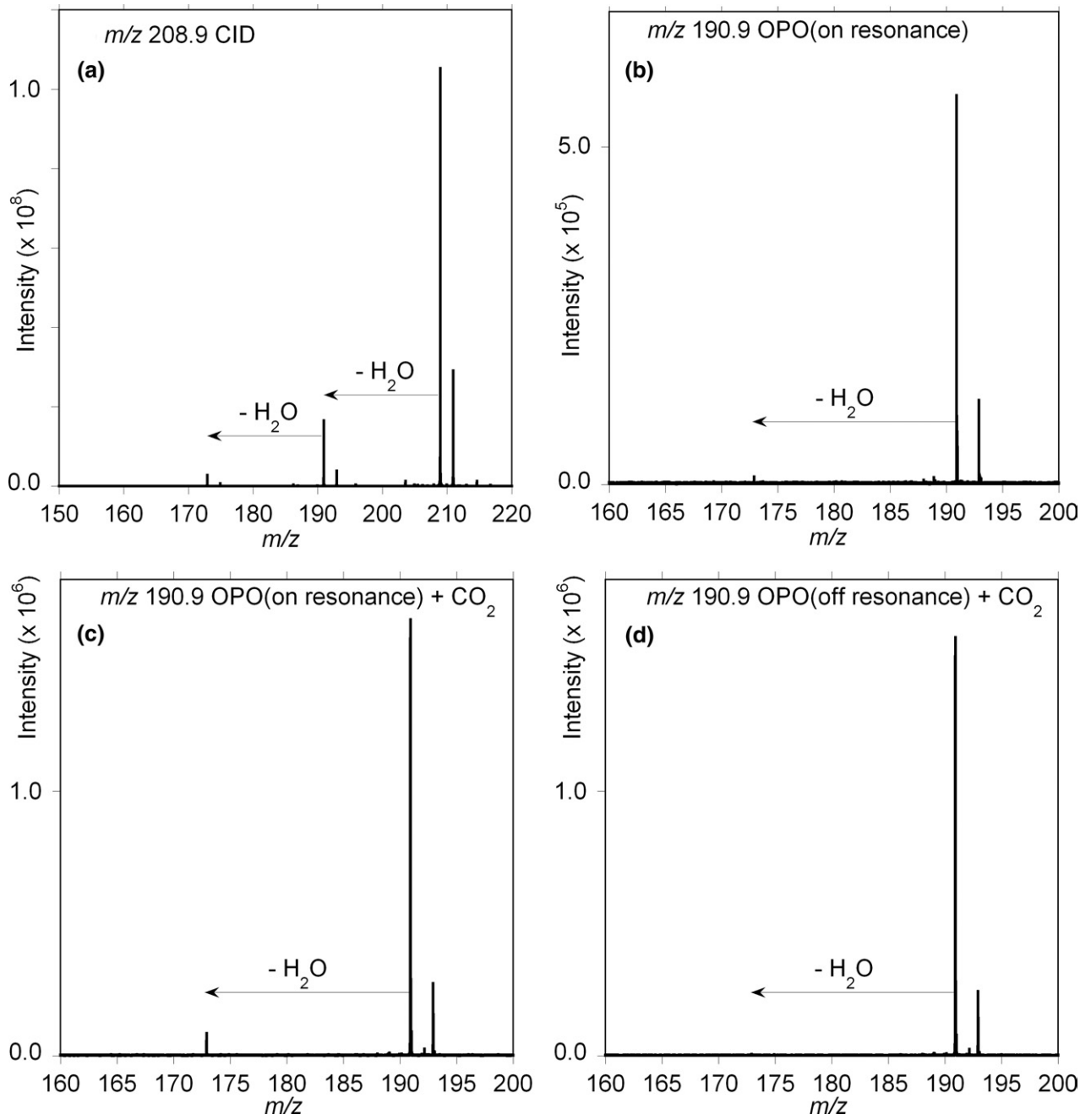

Figure 1. Collision induced dissociation (CID) mass spectrum of $[Mn(ClO_4)(H_2O)_3]^+$ (**a**) and IRMPD mass spectra of $[Mn(ClO_4)(H_2O)_2]^+$ recorded under different irradiation conditions (**b**)–(**d**): using only the OPO/OPA on resonance (3600 cm^{-1}) (**b**), using the CO_2 laser and the OPO/OPA on resonance (3600 cm^{-1}) (**c**), and using the CO_2 laser and the OPO/OPA off resonance (3450 cm^{-1}) (**d**).

bonds can be anticipated. In the case of the $Ni(H_2O)_n^+$ clusters, for example, IR spectroscopic evidence of the formation of structures with hydrogen bonds were found starting at $n = 4$ [22]. For metal dication $Ca(H_2O)_n^{2+}$ [18], there is no evidence for hydrogen bond formation for $n \leq 6$, but the marked changes in the IR spectrum for $n = 7$ was interpreted as the result of the formation of structures with hydrogen bonds between first and second shell water molecules. Depending on the nature of the water–water hydrogen bonds, the hydrogen-bonded OH stretching frequency can range from 3200 to 3800 cm^{-1}. The broad IR band observed at ~3500 cm^{-1} for $[Mn_2(ClO_4)_3(H_2O)_4]^+$ and $[Mn_2(ClO_4)_3(H_2O)_5]^+$ could thus be interpreted as a clear evidence of hydrogen bond formation.

As can seen in Figure 2b, a broad and weak signal in the same energy range can also be distinguished in the case of $n = 3$. It thus seems that there is a progressive increase of the signal at ~3500 cm^{-1} within the $[Mn_2(ClO_4)_3(H_2O)_n]^+$ series. In the case of

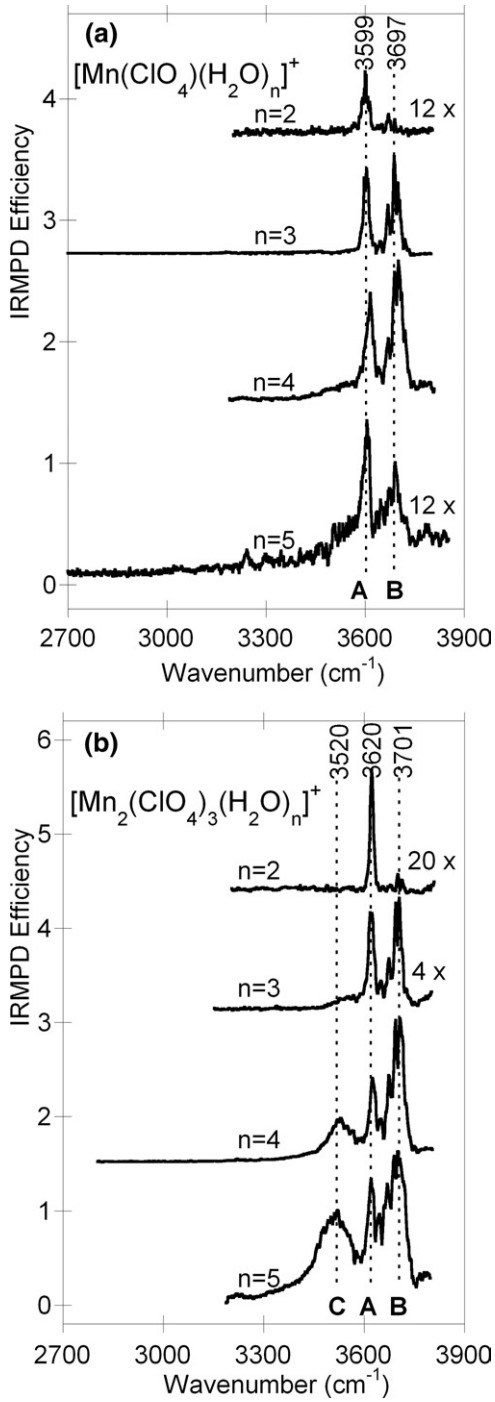

Figure 2. Experimental gas-phase infrared spectra of $[Mn(ClO_4)(H_2O)_{2-5}]^+$ (**a**) and $[Mn_2(ClO_4)_3(H_2O)_{2-5}]^+$ (**b**) cluster ions in the water O–H stretching region recorded with the combination of the OPO/OPA and CO_2 lasers. In part (**a**), dashed lines at 3599 and 3697 cm^{-1} show the position of bands A and B, respectively. In part (**b**), dashed lines at 3520, 3620, and 3701 cm^{-1} show the position of bands C, A, and B, respectively.

the $[Mn(ClO_4)(H_2O)_n]^+$, although there is no clear IR band in the 3200–3550 cm^{-1} energy range, one may see that a weak IR photofragmentation signal could be observed for $n = 5$ below 3600 cm^{-1} (Figure 2a). One may thus conclude that under our experimental conditions, a small fraction of the ions have a structure with water molecules involved in hydrogen bonds. Interestingly, in the case of $Ni(H_2O)_n^+$ clusters [22], it was suggested that bands observed near 3500 cm^{-1}, for n = 5–6 for example, are the signature of the OH stretches of water molecules involved in a hydrogen bond with the same double-acceptor (AA) hydrogen bond water molecule.

Formation of water–water hydrogen bonds within water solvated metal cluster ions can also be evidenced by changes in the free OH stretching region, [22] as also found for protonated water clusters [11]. The intensity of the symmetric OH stretch gradually diminishes while the asymmetric OH stretches develops into a closely spaced doublet near 3700 cm^{-1} as found in the case of $Ni(H_2O)_n^+$ clusters [22]. For small number of water molecules, however, a more complex multiplet structure is observed in the free OH stretching region, which is because different water molecules either directly bound to the metal or in the second coordination sphere. As can be seen in Figure 2b, it seems that the situation is somewhat similar in the case of the $[Mn_2(ClO_4)_3(H_2O)_n]^+$ clusters: for $n = 4$ and 5, while the band at ~3500 cm^{-1} increases, there is a clear decrease of the intensity of the symmetric OH stretch. This trend might be considered as an additional evidence of hydrogen bond formation for the larger bimetallic cluster ions.

Structures of the $[Mn(ClO_4)(H_2O)_{2-5}]^+$ Clusters

An exhaustive exploration of the potential energy surface of the $[Mn(ClO_4)(H_2O)_n]^+$ and $[Mn_2(ClO_4)_3(H_2O)_n]^+$ complexes for $n = 2$–5 is beyond the scope of this paper. Our goal is, rather, to determine the infrared signature of the different bonding motifs that can be anticipated for these cluster ions, and previously reported IR spectroscopic investigations of $Ni(H_2O)_n^+$ [22], $Ca(H_2O)_n^{2+}$ [18], and $Cs(H_2O)_n^+$ [12] provide a useful guide. We were especially interested in deriving the IR spectra of structures characterized by all the water molecules directly bound to the metal dication, and also those with water molecules in the second coordination shell. These two types of structures have been considered for the $[Mn(ClO_4)(H_2O)_n]^+$ cluster ions, and the optimized geometries are displayed in Figure 3 and the relative energies are given in Table 1.

The notation used hereafter for the different isomeric structures of the $[Mn(ClO_4)(H_2O)_n]^+$ cluster ions can be illustrated in the case of the $[Mn(ClO_4)(H_2O)_3]^+$ ions. The notation MnL_30 refers to structures in which the three water molecules are directly bound to the metal cation of the $[Mn(ClO_4)]^+$ core, and structures with one water molecule in the second shell of a dicoordinated Mn^{2+} are denoted as MnL_21. The water molecule in the second coordination sphere can be a single hydrogen bond acceptor (A), or a double hydrogen bond acceptor (AA), and the two corresponding optimized structures are denoted as MnL_21_A and MnL_21_AA,

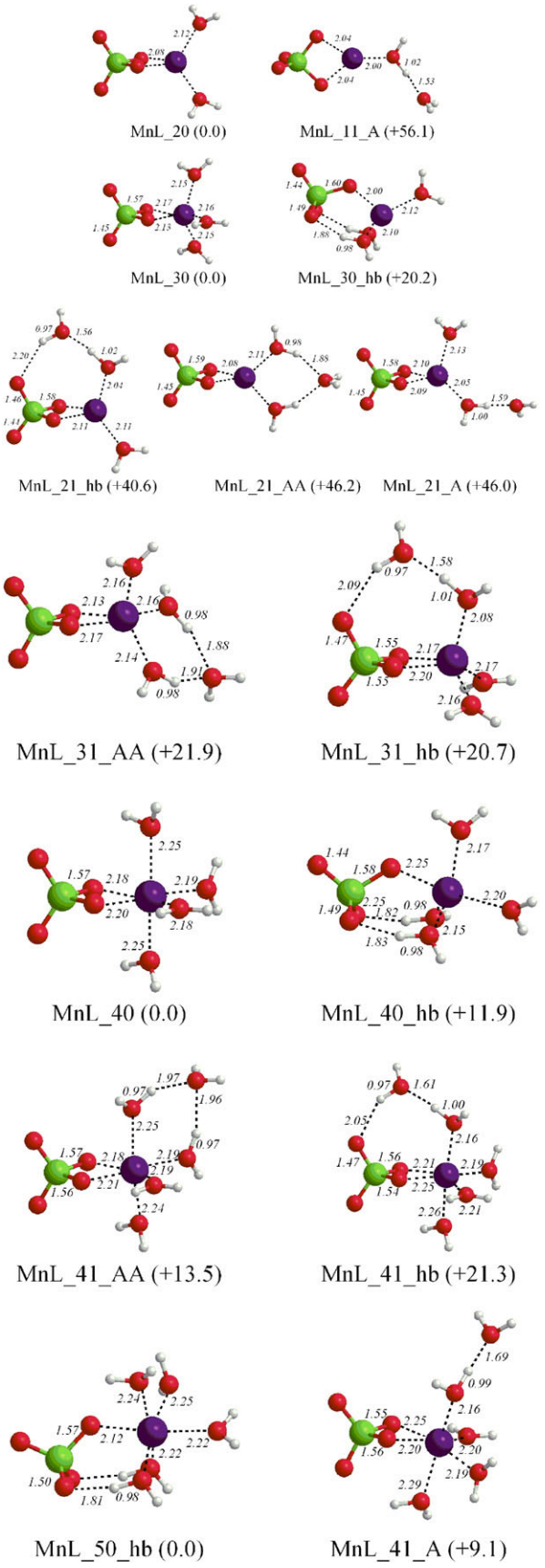

Figure 3. Representative structures for the $[Mn(ClO_4)(H_2O)_n]^+$ (n = 2–5) clusters (see text for the nomenclature). Relative MP2 0 K enthalpies (kJ/mol) are given in parentheses. Bond lengths are given in Å.

Table 1. Computed relative 0 K enthalpies and 298 K free enthalpies (in kJ/mol) for various isomers (see Figure 3) of $[Mn(ClO_4)(H_2O)_n]^+$ (n = 2–5) using both the B3LYP/6-311+G(d,p) and MP2/6-311+G(d,p) methods. The B3LYP enthalpy and entropy corrections were used for deriving the MP2 values

	UMP2 Rel. H0	B3LYP Rel. H0	UMP2 Rel. G298	B3LYP Rel. G298
MnL_11	56.1	41.8	57.2	42.9
MnL_20	0.0	0.0	0.0	0.0
MnL_21_A	46.0	30.7	41.6	26.3
MnL_21_AA	46.2	30.2	50.2	34.2
MnL_21_hb	40.6	28.5	41.9	29.8
MnL_30_hb	20.2	14.0	23.0	16.7
MnL_30	0.0	0.0	0.0	0.0
MnL_31_AA	21.9	9.1	20.0	7.2
MnL_31_hb	20.7	4.6	20.7	4.6
MnL_40_hb	11.9	1.5	15.8	5.4
MnL_40	0.0	0.0	0.0	0.0
MnL_41_A	21.3	14.0	10.3	3.3
MnL_41_AA	13.5	5.2	8.0	0.3
MnL_41_hb	9.1	3.9	4.9	0.0
MnL_50_hb	0.0	0.0	0.0	0.3

respectively. As can be seen in Figure 3, a third structure with one water molecule in the second coordination sphere could be characterized. This structure (MnL_21_hb) is characterized by a hydrogen bond between a water molecule and a perchlorate oxygen. Finally, when the three water molecules are directly bound to Mn^{2+}, a structure denoted as MnL_30_hb characterized by a hydrogen bond between a water molecule and a perchlorate oxygen was also optimized.

The most stable geometries for $[Mn(ClO_4)(H_2O)_n]^+$ (n = 2–5) complexes were found to correspond to structures in which all the water molecules are directly bound to Mn(II) of the $[Mn(ClO_4)]^+$ core (see Table 1). Except in the case of the lowest energy structure of $[Mn(ClO_4)(H_2O)_5]^+$, which will be discussed below, the most favorable coordination mode of the perchlorate was found to be η^2. For n = 2, this leads to a coordination number (CN) of four for Mn(II). While one could conceive that for these low coordination complexes, the perchlorate ligand could adopt an η^3 coordination mode, thereby leading to a formal coordination number of 5 and 6 for $[Mn(ClO_4)(H_2O)_2]^+$ and $[Mn(ClO_4)(H_2O)_3]^+$, respectively, no such minimum was found on the potential energy surface of these complexes. Attempts for characterizing structures with a η^3 perchlorate and thus a CN of five failed, and the geometry optimization led to an η^2 perchlorate. For n = 3 and 4, two structures characterized by a different coordination mode of the perchlorate were characterized. In these two cases, the lowest energy structure (MnL_30 and MnL_40) has no hydrogen bonds and the coordination mode of the perchlorate is η^2, leading to a CN mode of five and six, respectively.

A higher energy structure (MnL_30_hb and MnL_40_hb) characterized by two water–perchlorate hydrogen bonds was optimized in the two cases. The optimized

MnL_40_hb structure (Figure 3) can be considered as a pseudo trigonal bipyramidal structure with a distorted η^1 perchlorate allowing for the formation of two hydrogen bonds between two pseudo-equatorial water molecules and two perchlorate oxygen atoms, as evidenced by the relatively short distance (~1.82–1.83 Å) between the perchlorate oxygen and the water hydrogen atoms. Formation of these two hydrogen bonds is also characterized the lengthening of the associated OH (~+0.02 Å) bonds. The geometrical features of the hydrogen bonds of the MnL_30_hb structures are essentially similar. Most importantly, the corresponding optimized bond lengths were found to be similar at both B3LYP and MP2 levels.

Interestingly, the formation of these water–perchlorate hydrogen bonds within the first coordination sphere of Mn(II) is accompanied by an η^2 to η^1 change of the coordination mode of the perchlorate thus reducing the CN of Mn(II). It should be noted that in the case of the $[Mn(ClO_4)(H_2O)_5]^+$ clusters, the η^2 to η^1 change of the coordination mode of the perchlorate is mandatory to accommodate five water molecules in the first coordination shell of Mn(II) leading to a hexacoordinated Mn^{2+} ion. The resulting MnL_5_hb structure was found to be the lowest energy structure for $[Mn(ClO_4)(H_2O)_5]^+$. In the cases of $[Mn(ClO_4)(H_2O)_3]^+$ or $[Mn(ClO_4)(H_2O)_4]^+$, one could also imagine another distortion of the η^2 (towards the η^3 coordination) allowing for the formation of a single water-perchlorate, but keeping formally the CN of Mn(II) constant. Nevertheless, attempts to optimize such a structure for $[Mn(ClO_4)(H_2O)_3]^+$ led to an MnL_30 type structure.

As the number of water molecules increases, one would expect structures with one water molecule in the second coordination shell to be more and more favorable. While this trend is observed at both B3LYP and MP2 levels (see Table 1), it is important to stress that these structures are predicted to be lower in energy at the B3LYP than at the MP2 level. On the basis of extensive theoretical studies of metal aqua ions [46], and of the particular case of $[Mn(H_2O)_n]^{2+}$ complexes [47], likely the relative energies of hydrogen bonded structures are underestimated at the B3LYP level, and the MP2 relative energies can be considered as more reliable.

Three types of isomers with one water molecule in the second coordination sphere of Mn(II) were characterized. As illustrated in the case of the $[Mn(ClO_4)(H_2O)_n]^+$ (n = 3–5) clusters, it is energetically favorable to have the second shell water molecule forming a bridge between a first shell water molecule and a perchlorate oxygen. It should be noted, however, that the corresponding distance between the water hydrogen and the perchlorate oxygen is relatively long and decreases when n increases (~2.20, ~2.09, and ~2.05 Å for n = 3, 4, and 5, respectively). This suggests that the formation of the cyclic hydrogen bond is easier when the single-donor water molecule is cis to the perchlorate. In the case of $[Mn(ClO_4)(H_2O)_2]^+$, however, no such minimum could be found on the PES, which is probably because the relatively weak hydrogen bond does not compensate for the energetic cost associated with the deformation of the first coordination shell required for the formation of the cyclic hydrogen bonding network.

Structures with a single-acceptor (A) or a double-acceptor (AA) water molecule in the second shell were also characterized for the $[Mn(ClO_4)(H_2O)_n]^+$ clusters. As illustrated in the cases of n = 3 and 5 (see Table 1), the former are higher in energy than the latter. On the other hand, as can be seen in Table 1, structures with a double-acceptor (AA) water molecule are consistently found to be slightly higher in energy than those having the second shell water molecule forming a bridge between a first shell water molecule and a perchlorate oxygen.

From the calculated energies of the various structures of the $[Mn(ClO_4)(H_2O)_n]^+$ (n = 2–5) clusters, one would expect that the most abundant isomers formed under our gas-phase experimental conditions have all the water molecules in the first coordination sphere. Structures with one water molecule in the second coordination sphere are higher in energy, the energy gap decreasing with the cluster size. From the computed relative energies, however, it is conceivable that these latter structures could be formed for the largest cluster size. Indeed, as can be seen in Table 1, if one considers the relative ΔG(298K), MnL_41_hb is predicted to be the lowest energy structure for the $[Mn(ClO_4)(H_2O)_5]^+$ cluster at the B3LYP level, and it is only 4.9 kJ/mol higher in energy than the MnL_50_hb at the MP2 level of theory.

IR spectra of the $[Mn(ClO_4)(H_2O)_n]^+$ (n = 2–5) clusters in the OH stretching region will be analyzed in a subsequent section, but we will first discuss the IR spectra in the 800–1700 cm^{-1} region, which also provide useful information on the coordination mode of the perchlorate ligand.

Coordination Mode of the Perchlorate Ligand: IR Spectra of the $[Mn(ClO_4)(H_2O)_{2-3}]^+$ Clusters in the 800–1700 cm^{-1} Spectral Range

The IRMPD spectra recorded in the 800–1700 cm^{-1} spectral range for the $[Mn(ClO_4)(H_2O)_2]^+$ and $[Mn(ClO_4)(H_2O)_3]^+$ cluster ions are given in Figure 4. While larger size clusters either containing an $[Mn_2(ClO_4)_3]^+$ core and/or more water molecules could be easily isolated using the 7 tesla FTICR ion trap, only $[Mn(ClO_4)(H_2O)_2]^+$ and $[Mn(ClO_4)(H_2O)_2]^+$ could be trapped using the quadrupole ion trap, which was the only tandem mass spectrometer available when the IR beam was available. As already reported for another investigation of the hydrated ion-pair $[Mg(NO_3)(H_2O)_n]^+$ system [39], the water partial pressure in the ion trap is such that reactions take place between the complexes and water molecules at the timescale of the experiment.

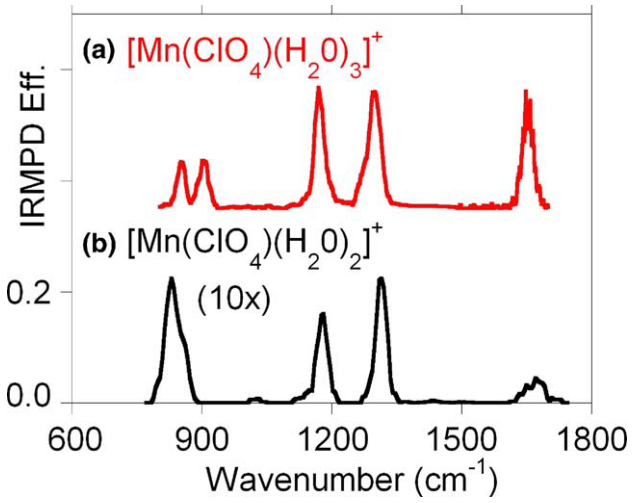

Figure 4. Experimental gas-phase infrared spectra of $[Mn(ClO_4)(H_2O)_3]^+$ (**a**), and $[Mn(ClO_4)(H_2O)_2]^+$ (**b**), cluster ions in the 800–1800 cm^{-1} mid-infrared region. The vertical scale is the IRMPD fragmentation efficiency.

In the case of $[Mn(ClO_4)(H_2O)_3]^+$, five IRMPD bands are observed in the spectral range investigated. The central frequency of these bands is ~854 cm^{-1}, ~986 cm^{-1}, ~1172 cm^{-1}, ~1300 cm^{-1}, and ~1652 cm^{-1}. As can be seen in Figure 4, the IRMPD spectrum of $[Mn(ClO_4)(H_2O)_2]^+$ shows similar features, although only four bands are observed at ~837 cm^{-1}, ~1179 cm^{-1}, ~1314 cm^{-1}, and ~1669 cm^{-1}. Interestingly, the IRMPD band observed at ~837 cm^{-1} is quite broad (FWHM ~50 cm^{-1}) compared with the other bands of $[Mn(ClO_4)(H_2O)_2]^+$ or the bands of $[Mn(ClO_4)(H_2O)_3]^+$ for which the bandwidth is about ~25 cm^{-1}, as usually observed under similar experimental conditions [40]. This may suggest that the band at ~837 cm^{-1} corresponds to two closely spaced IR absorption features of $[Mn(ClO_4)(H_2O)_2]^+$.

The experimental IRMPD spectrum of the $[Mn(ClO_4)(H_2O)_3]^+$ cluster ions is compared with the calculated IR absorption spectra of the five structures determined at the MP2 level in Figure 5. The five structures have very different IR absorption spectra in the 800–1700 cm^{-1} spectral range explored here. Inspection of Figure 5 clearly shows that the experimental IRMPD spectrum of the $[Mn(ClO_4)(H_2O)_3]^+$ cluster ions compares very well with the calculated IR absorption spectrum of the lowest energy structure MnL_30. Before assigning the five observed IRMPD bands, we would like to discuss the relative performance of the B3LYP and MP2 levels for predicting the IR absorption spectrum of this structure of $[Mn(ClO_4)(H_2O)_3]^+$ in the 800–1700 cm^{-1} spectral range.

Three types of vibrational modes have large IR cross section in the 800–1700 cm^{-1} spectral range. Water bending modes are expected at ~1650 cm^{-1}. Second, the four perchlorate Cl–O stretches should also be associated with large IR cross-section in this spectral range. Finally, in the case of hydrogen bonded structures, water OH bending modes associated with hydrogen donors are also predicted to have large IR cross-section. Harmonic frequencies have been determined at both B3LYP and MP2 level of theory for the five structures of the $[Mn(ClO_4)(H_2O)_3]^+$ cluster ions. In each case, the two calculated IR absorption spectra were found to be very different. This is illustrated in Table 2, where the results associated with the MnL_30 structure are summarized. As can be seen in Table 2, the frequencies of the four Cl–O stretches calculated at the two levels of theory are significantly different. While the predicted frequencies for the water bending modes are rather similar at the B3LYP and MP2 levels, the calculated frequencies of the Cl-O stretches are significantly smaller at the B3LYP than at the MP2 level.

To understand these differences of Cl–O stretching frequency calculated at the B3LYP and MP2 levels, harmonic frequencies have been systematically calculated for ClO^-, ClO_2^-, ClO_3^-, and ClO_4^- free anions, and the same conclusions can be made: the B3LYP Cl-O

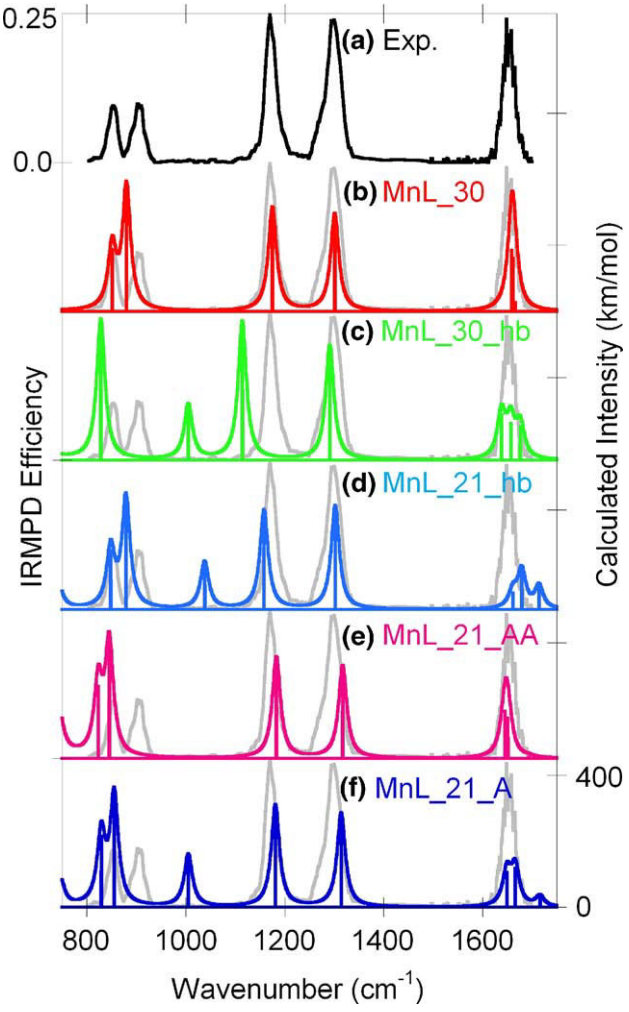

Figure 5. Infrared spectra of $[Mn(ClO_4)(H_2O)_3]^+$ in the 800–1800 cm^{-1} mid-infrared region. The experimental IRMPD spectrum (**a**) is compared with MP2 calculated spectra for five different bonding motifs (**b**)–(**f**).

Table 2. Experimental and calculated frequencies (in cm^{-1}) of ClO_2^-, $[Mn(ClO_4)(H_2O)_2]^+$, and $[Mn(ClO_4)(H_2O)_3]^+$. Unscaled harmonic frequency values calculated at the B3LYP and MP2 level using the 6-311+G(d,p) basis set are tabulated

	ClO_2^-				
IR mode	Ar Matrix IR[a]		MP2		B3LYP
ClO sym st.	790		841		689
ClO as. St.	823		866		729
	$[Mn(ClO_4)(H_2O)_2]^+$				
		MnL_20		MnL_11_A	
IR mode	IRMPD[b]	MP2	B3LYP	MP2	B3LYP
ClO sym st.[c]	837	821	703	804	689
ClO as st.[c]		845	744	826	726
OH bending				1067	1067
ClO sym st.	1179	1186	1057	1194	1062
ClO as st.	1314	1324	1185	1340	1198
	$[Mn(ClO_4)(H_2O)_3]^+$				
		MnL_30		MnL_21_A	
IR mode	IRMPD[b]	MP2	B3LYP	MP2	B3LYP
ClO sym st.[c]	854	851	736	829	712
ClO as st.[c]	906	880	780	855	758
OH bending				1005	988
ClO sym st.	1172	1175	1047	1182	1053
ClO as st.	1300	1301	1165	1315	1176

[a]From reference [52].
[b]This work.
[c]Symmetric and antisymmetric combinations of the two Cl–O stretches involving oxygen atoms bound to Mn(II).

stretching frequencies are significantly smaller than those calculated at the MP2 level, the B3LYP/MP2 frequency ratio ranging from 0.82 to 0.89. The IR spectrum of ClO_2^- has been determined in Ar matrix conditions, [52] and the symmetric and antisymmetric Cl–O stretching frequencies were reported at 790 and 823 cm^{-1}. As can be seen in Table 2, the two calculated B3LYP frequency values (689 and 729 cm^{-1}) are lower than those observed experimentally, with an experimental/calculated ratio of 1.14. On the other hand, the harmonic frequencies determined at the MP2 level are slightly larger the corresponding values determined experimentally, with an experimental/calculated ratio value of 0.95. While the Cl–O stretching frequencies are unexpectedly underestimated at the B3LYP level, it seems that the average scaling factor value (0.95) determined for the MP2 Cl–O stretching frequencies can be considered as reasonable, and the MP2 calculated IR absorption spectra will be used for the spectral assignment in the 800–1700 cm^{-1} spectral range.

With these conclusions in mind, an assignment of the IRMPD bands observed for $[Mn(ClO_4)(H_2O)_2]^+$ and $[Mn(ClO_4)(H_2O)_3]^+$ can be made. The bands observed at ~1650–1670 cm^{-1} can be safely assigned to the water bending modes. Assuming that the most of the ions formed under our experimental conditions have the lowest energy MnL_30 structure with all the water molecules directly bound to the Mn^{2+}, the agreement between the positions of the bands in the lower wave number part of the IRMPD spectrum and the MP2 calculated IR absorption spectrum is rather good. As can be seen in Table 2, the experimental/MP2-calculated frequency ratio is about 1.00 for the four observed IRMPD bands corresponding with the Cl–O stretches. Formation of hydrogen bond between perchlorate oxygens and the water molecules of the first coordination shell as in structure MnL_30_hb is accompanied by an $\eta^2 \rightarrow \eta^1$ coordination change of the perchlorate. This strongly affects the Cl–O stretching modes, and thereby the IR absorption spectrum in the 800–1400 cm^{-1} spectral range for the $[Mn(ClO_4)(H_2O)_3]^+$ complex (see Figure 5). The fact that no strong IR features is observed between 900 and 1100 cm^{-1} suggests that no hydrogen bond is formed between perchlorate oxygens and the water molecules of the first coordination shell since the predicted IR absorption spectrum of MnL_30_hb structure has a relatively strong IR absorption feature (calculated intensity ~160 km/mol) at 1005 cm^{-1}.

The analysis of the normal modes of the IR active bands of the structures presenting a water molecule in the second solvation sphere of manganese reveals that two types of vibrational modes are at play in the 600–1400 cm^{-1} spectral range. Besides the Cl–O stretches, out of plane OH–O bending modes also have strong IR cross-section. In the cases of MnL_21_hb and MnL_21_A structures, the Cl–O stretches are relatively unchanged compared with the MnL_30 structures, but they have an additional IR absorption band at ~1000–1050 cm^{-1} corresponding to an out of plane OH–O bending. The fact that no IR photodissociation signal is observed in this region suggests that these two structures are not formed under our experimental conditions. It should also be noted that the hydrogen bond formation in MnL_21_hb and MnL_21_A induces a degeneracy splitting of the water bending mode. This is also consistent with the fact that these structures are not populated since their water bending absorption band is broad while the observed band is quite narrow.

The calculated IR absorption spectrum of the MnL_21_AA structure, on the other hand, does not strongly differ from the one of the MnL_30 structure. As in the case of the other two structures (MnL_21_A and MnL_21_hb) with a water molecule in the second shell, the Cl–O stretches are nearly at the same frequencies. In contrast with structures MnL_21_A and MnL_21_hb, however, the out of plane OH–O bending modes are predicted at lower frequencies (627 and 738 cm^{-1}) for the MnL_21_AA structure. It is therefore more difficult to rule out the formation of structure with a double-acceptor water molecule under our experimental conditions on the sole basis of the IR spectrum of MnL_21_AA. Considering its relative energy (30.2 and 40.5 at the B3LYP and MP2 level, respectively) with respect to the MnL_30, however, it seems very unlikely that such $[Mn(ClO_4)(H_2O)_3]^+$ structure is present in our experiment.

As a conclusion, the bands observed in the 800–1400 cm^{-1} energy range for both $[Mn(ClO_4)(H_2O)_2]^+$ and $[Mn(ClO_4)(H_2O)_3]^+$ complexes allow for a clear characterization the η^2 coordination mode of the perchlorate ligand. The symmetric and antisymmetric combinations of the two Cl–O stretches associated with the oxygen bound to the manganese are found red-shifted compared with the corresponding "free Cl–O" stretches (see Table 2). As can be seen in Table 2, the splitting between the two "bound Cl–O" stretches is predicted to be small at the MP2 level (24 cm^{-1} and 29 cm^{-1} in the case of $[Mn(ClO_4)(H_2O)_2]^+$ and $[Mn(ClO_4)(H_2O)_3]^+$, respectively), and of the same magnitude as the bandwidth (25 cm^{-1}) of the IRMPD bands, which might explain that only one broad feature was observed for $[Mn(ClO_4)(H_2O)_2]^+$ at 837 cm^{-1}.

IR Spectra of the $[Mn(ClO_4)(H_2O)_{2-5}]^+$ Clusters in the OH Stretching Region

The IR spectra of the $[Mn(ClO_4)(H_2O)_n]^+$ (n = 2–5) cluster ions recorded in the OH stretching region (Figure 2) display two strong IR features in this spectral range. This strongly suggests that the structures formed under our experimental conditions do not have any strong hydrogen bonds involving a water molecule, which should be characterized by a strongly red-shifted OH stretching mode. This is supported by the following comparison of the experimental IR spectra with the computed IR spectra of the different low-energy lying structures in the cases of the $[Mn(ClO_4)(H_2O)_3]^+$ and $[Mn(ClO_4)(H_2O)_5]^+$ cluster ions.

The experimental IR spectrum of the $[Mn(ClO_4)(H_2O)_3]^+$ ions has been recorded in the 2650–3800 cm^{-1} spectral range. In Figure 6, this experimental IR spectrum is compared with the computed IR absorption spectra of the four optimized structures (MnL_30, MnL_30_hb, MnL_21_hb, and MnL_21) determined at the B3LYP level of theory. The calculated harmonic frequencies have been scaled by a factor of 0.96, and the IR absorption cross sections shown in Figure 6 have been obtained assuming that each calculated IR band has a Lorentzian profile (FWHM = 20 cm^{-1}). As can be seen in Figure 6, the experimental IR spectrum nicely matches with the calculated IR spectrum of the lowest-energy MnL_30 structure. As expected, the two bands observed at ~3605 and ~3690 cm^{-1} correspond to the symmetric and antisymmetric combinations of the OH stretching modes which are predicted at ~3595 and ~3687 cm^{-1} at the B3LYP level for the MnL_30 structure.

Formation of $[Mn(ClO_4)(H_2O)_3]^+$ ions with one water molecule in the second coordination sphere is very unlikely. This can be concluded from the comparison of the IR absorption spectrum of two such representative MnL_21 and MnL_21_hb structures with the experimental IR spectrum. Whereas no IR photofragmentation signal could be observed below 3000 cm^{-1}, these

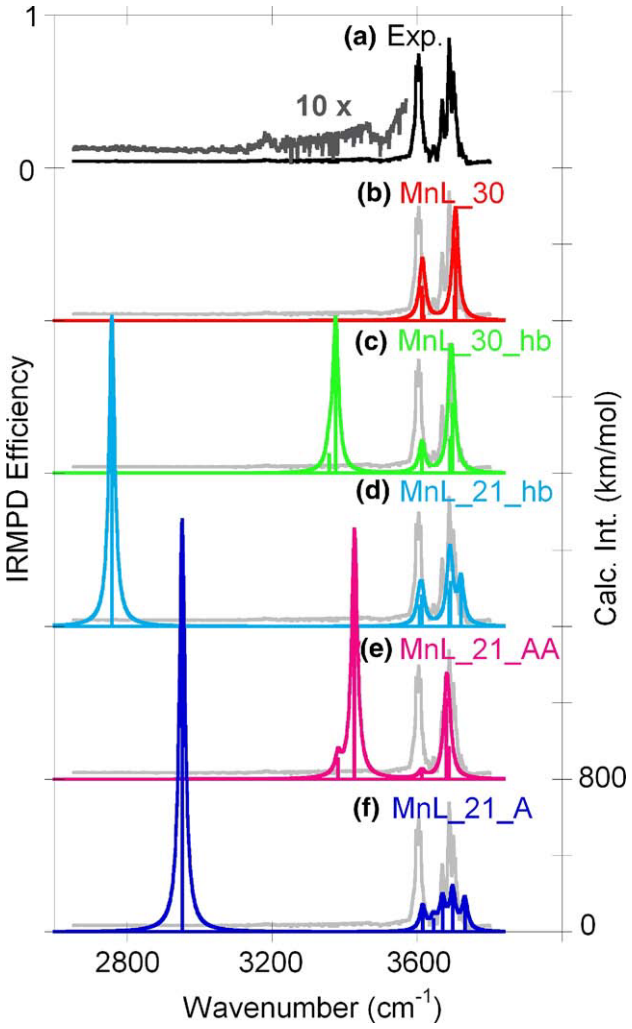

Figure 6. Infrared spectra of $[Mn(ClO_4)(H_2O)_3]^+$ in the water OH stretching region. The experimental IRMPD spectrum (**a**) is compared with B3LYP calculated spectra for five different bonding motifs **(b)–(f)**.

two structures share the same type of IR signature: a strongly IR active band corresponding to a red-shifted OH stretch associated with a hydrogen bond donor water molecule. This band is predicted 2742 and 2945 cm^{-1}, with an intensity of 1623 and 2157 km/mol, for structures MnL_21_hb and MnL_21, respectively. For large size water solvated metal cluster cations, it has been shown that these red-shifted water OH stretching modes give rise to broad bands [22, 26]. In the present case, however, there is no trace of photofragmentation below 3000 cm^{-1}. One can thus conclude that no $[Mn(ClO_4)(H_2O)_3]^+$ ions with one water molecule in the second coordination shell is formed under our experimental conditions.

On the other hand, a very weak and broad signal can be observed between 3000 and 3500 cm^{-1}. On the basis of the exploration of the potential energy surface of the $[Mn(ClO_4)(H_2O)_3]^+$ ions, one could conclude that structures such as MnL_30_hb are formed. At the two levels of theory considered here, the MnL_30_hb structure is

predicted to be only ~14 kJ/mol above the lowest-energy MnL_30 structure. The MnL_30_hb structure is characterized by a hydrogen bonding between perchlorate oxygens and water molecules in the first coordination shell. As can be seen in Figure 6, this type of hydrogen bonds has a clear IR signature: the OH stretching frequencies of the single donor (D) water molecules are predicted at 3340 and 3358 cm^{-1} and have a relatively large calculated intensities (97 and 797 cm^{-1}, respectively). This could give rise to the very broad IR photodissociation signal observed between 3000 and 3500 cm^{-1}.

As discussed in the previous section, the IR absorption spectra calculated at the B3LYP and MP2 levels differ significantly in the Cl–O stretching region. On the other hand, the two sets of calculated spectra are rather similar in the OH stretching region. This is illustrated in the case of the $[Mn(ClO_4)(H_2O)_3]^+$ ions. The calculated IR absorption spectra for the low-energy structures at the B3LYP and MP2 levels are provided in Figure 6 and Supplemental Figure S2, respectively, (Supplemental Information can be found in the electronic version of this article). The largest difference between the sets of calculated spectra is found in the case of MnL_30_hb. As mentioned just above, at the B3LYP level, the frequency splitting between the red-shifted OH stretching modes of the two single donor water molecules is small (18 cm^{-1}), and the symmetric combination is about ten times more IR active than the antisymmetric combination. At the MP2 level, however, the predicted intensities are nearly the same (~380 km/mol) and the frequency splitting is large (85 cm^{-1}). It may be interesting to notice that this difference between the OH stretching B3LYP and MP2 frequencies is only found when the corresponding water molecules are involved in hydrogen bonds with perchlorate oxygens, and may thus be correlated with the significant difference in the description of the Cl–O stretches at the MP2 and B3LYP levels.

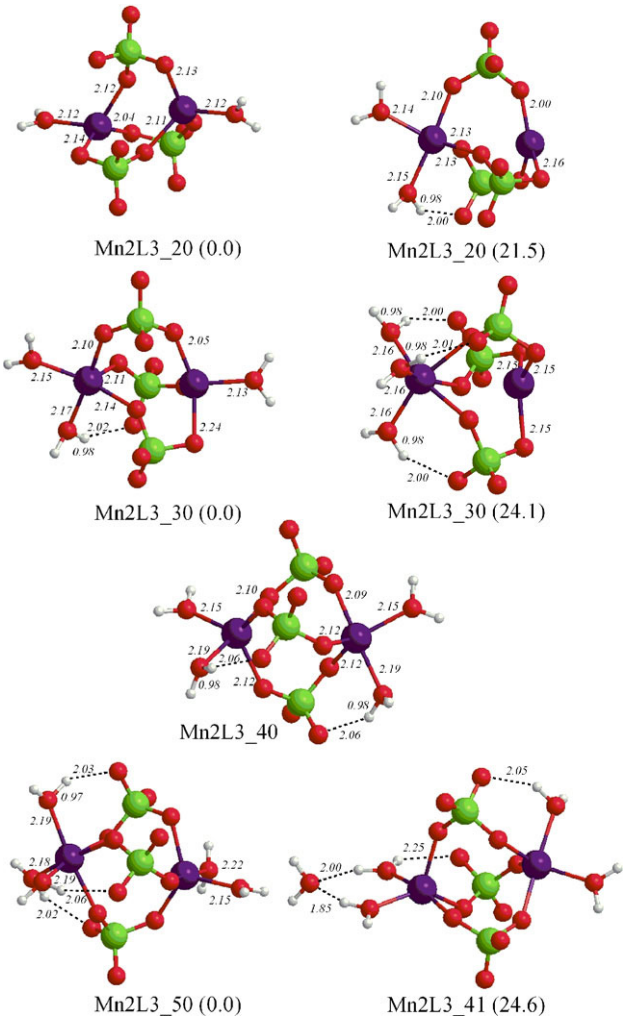

Figure 7. Structures for the $[Mn_2(ClO_4)_3(H_2O)_n]^+$ (n = 2–5) clusters (see text for the nomenclature). Relative B3LYP OK enthalpies (kJ/mol) are given in parentheses. Bond lengths are given in Å.

IR Spectra of $[Mn_2(ClO_4)_3(H_2O)_{2-5}]^+$ Clusters in the OH Stretching Region

All the structures considered for the $[Mn_2(ClO_4)_3(H_2O)_{2-5}]^+$ cluster ions are based on an $[Mn_2(ClO_4)_3]^+$ core where the three perchlorate ligands bridge across the two metal centers. No highly symmetric minimum could be found for the $[Mn_2(ClO_4)_3]^+$ system. The search for a minimum led to a highly distorted structure with C_1 symmetry. In this structure, an oxygen atom of each perchlorate is bound to each metal center, and the three corresponding Mn–O bond lengths are 2.00, 2.08, and 2.10 Å (Figure 7). One can thus consider that the coordination number of each Mn(II) in $[Mn_2(ClO_4)_3]^+$ is three, each metal center having a distorted planar trigonal environment. Starting from this $[Mn_2(ClO_4)_3]^+$ core structure, only a selected set of structures of the $[Mn_2(ClO_4)_3(H_2O)_{2-5}]^+$ clusters have been considered to propose an assignment of their IR features. This selection is based on the analysis of the relative energies of the $[Mn(ClO_4)(H_2O)_n]^+$ (n = 2–5) structures with different bonding motifs, and also on the comparison of the corresponding calculated spectra with experimental IR spectra.

When all the water molecules were considered to be directly bound to an Mn(II), the $[Mn_2(ClO_4)_3(H_2O)_2]^+$ structures with water molecules evenly distributed over the two metal centers were found to be lower in energy. In the case of $[Mn_2(ClO_4)_3(H_2O)_2]^+$, for example, the Mn2L3_20_b structure with two water molecules bound to a single metal atom was found to be significantly higher in energy (+21.5 kJ/mol) than the Mn2L3_20_a with one water molecule bound to each Mn(II). Similarly, the Mn2L3_30_b structure of $[Mn_2(ClO_4)_3(H_2O)_3]^+$ with three water molecules on the same manganese atom is also found significantly higher in energy (24.1 kJ/mol) than Mn2L3_30_a with two waters on one Mn(II) and one water on the other. On the basis of these results,

only the structures with two Mn(II) with a CN of five were considered for $[Mn_2(ClO_4)_3(H_2O)_4]^+$. Similarly, for $[Mn_2(ClO_4)_3(H_2O)_5]^+$, structures with one Mn(II) with a CN of 6 and the other with a CN of five were considered.

Hydrogen bonding between one water molecule of the first shell and a perchlorate oxygen was found to be favorable only when at least two water molecules were bound on an Mn(II) center. As said above, the coordination number of each Mn(II) is four for the lowest energy Mn2L3_20_a structure of $[Mn_2(ClO_4)_3(H_2O)_2]^+$ (Figure 7). Each metal center has a distorted tetrahedral geometry, but there is no structural evidence for hydrogen bonding within the first shell. When the two water molecules of $[Mn_2(ClO_4)_3(H_2O)_2]^+$ are considered to be bound on the manganese, geometry optimization leads to an Mn2L3_20_b structure, where the penta-coordinated Mn has a pseudo trigonal bipyramidal environment with one water molecule in axial position. As can be seen in Figure 7, hydrogen bonding occurs between this water molecule and a perchlorate oxygen, and the corresponding H–O hydrogen bond distance is ~2.00 Å. A similar hydrogen bonding distance (~2.02 Å) is found in the lowest energy Mn2L3_30_a structure of $[Mn_2(ClO_4)_3(H_2O)_3]^+$, and it is interesting to note that this hydrogen bonding also involves the pseudo-axial water molecule of the pseudo-trigonal pyramidal Mn(II) center. The same type of hydrogen bonding motif is found in the Mn2L3_40 structure of $[Mn_2(ClO_4)_3(H_2O)_4]^+$ displayed in Figure 7, although the corresponding hydrogen bond distances are slightly longer (2.06 Å). In all cases, no hydrogen bond is formed between the pseudo-equatorial water molecule and a perchlorate oxygen.

Optimized structures with three water molecules on the same metal center are characterized by a hydrogen bond between each of these water molecules and a perchlorate oxygen. This situation is found, for example, in the high-energy Mn2L3_30_b structure of $[Mn_2(ClO_4)_3(H_2O)_3]^+$, and the three hydrogen bond H–O distances are relatively short (2.00–2.01 Å). The same hydrogen bonding motif is found in the lowest energy Mn2L3_50 structure of $[Mn_2(ClO_4)_3(H_2O)_5]^+$. There are three water–perchlorate hydrogen bonds within the first shell of the hexacoordinated Mn(II). On the other hand, no such hydrogen bond is formed between the ligands of the pentacoordinated Mn(II) center of the Mn2L3_50 structure (Figure 7). While we cannot rule out the existence of other isomers of $[Mn_2(ClO_4)_3(H_2O)_5]^+$ with another water–perchlorate hydrogen bonding motif, likely they should have similar IR features to the Mn2L3_50 structure shown in Figure 7.

Clusters with water molecules in the second shell are more likely to be formed for large size clusters, and they were therefore investigated in the case of the $[Mn_2(ClO_4)_3(H_2O)_5]^+$ cluster. On the basis of our results on $[Mn(ClO_4)(H_2O)_n]^+$ clusters, structures with a double-acceptor water molecule or a single-acceptor water molecule can be considered. In the later case, depending on whether the second shell water molecule forms a bridge or not through a hydrogen bond with a perchlorate oxygen, two types of isomers could be formed. As discussed above in the case of the $[Mn(ClO_4)(H_2O)_3]^+$ cluster, these two types of structures with a single-acceptor in the second shell have a distinct IR signature below ~3000 cm^{-1} corresponding to a strongly red-shifted OH stretching mode associated with the water–water hydrogen bond. Since no IR photodissociation signal could be observed below 3500 cm^{-1} for the $[Mn_2(ClO_4)_3(H_2O)_{4-5}]^+$ clusters (Figure 8), structures with a single-acceptor water molecule were not considered further.

Structures with a double-acceptor water molecule in the second shell, on the other hand, could be interesting candidate for the spectral assignment of the $[Mn_2(ClO_4)_3(H_2O)_n]^+$ clusters. On the basis of our results on the $[Mn(ClO_4)(H_2O)_n]^+$ clusters, they have two slightly red-shifted OH stretching modes associated with the single-donor water molecule that could account for the signal observed at ~3600 cm^{-1} in the cases of the $[Mn(ClO_4)(H_2O)_{4-5}]^+$ clusters. A corresponding structure (Mn2L3_41_AA) has been optimized for $[Mn_2(ClO_4)_3(H_2O)_5]^+$. As can be seen in

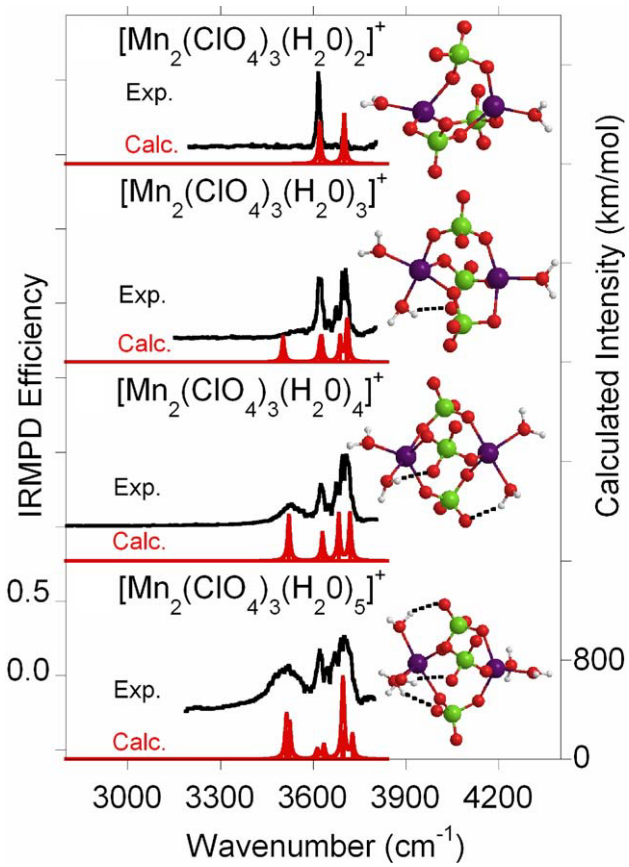

Figure 8. Infrared spectra of $[Mn_2(ClO_4)_3(H_2O)_n]^+$ (n = 2–5) in the water OH stretching region. For each cluster size (n), the calculated IR spectrum for the lowest-energy structure is compared with the corresponding experimental spectrum.

Figure 7, it was found to be significantly higher in energy (+24.6 kJ/mol at the B3LYP level) than the Mn2L3_50 structure. Considering that the stability of hydrogen bonded structures with respect to structures with all the water molecules in the first coordination shell is likely to be overestimated at the B3LYP, one may conclude that even for the largest $[Mn_2(ClO_4)_3(H_2O)_5]^+$ clusters studied here, structures with one second shell water molecule are high in energy.

In Figure 8, the gas-phase infrared spectra of the $[Mn_2(ClO_4)_3(H_2O)_n]^+$ (n = 2–5) clusters are compared with the calculated IR absorption spectrum of the lowest-energy structure. We will first discuss the broad and red-shifted band that is characteristic of hydrogen bonding. Overall, as can be seen in Figure 8, there is a good agreement between the experimental spectrum and calculated spectrum of the lowest energy structure in the region below 3600 cm^{-1}. Nevertheless, alternative structures with a double-acceptor water molecule may be at play. In the case of $[Mn_2(ClO_4)_3(H_2O)_5]^+$ the calculated spectrum of the corresponding Mn2L3_41_AA structure, along with that of the lowest energy Mn2L3_50 structure, is provided in Figure 9.

In the case of $[Mn_2(ClO_4)_3(H_2O)_5]^+$, the relatively broad feature characteristic of hydrogen bonding is observed at ~3520 cm^{-1} As can be seen in Figure 9, both Mn2L3_50 and Mn2L3_41_AA structures have IR bands in the 3400–3600 cm^{-1} frequency range. In the case of Mn2L3_50, the three water–perchlorate hydrogen bonds are nearly equivalent, and the three normal modes associated with the single-donor water OH stretches are nearly degenerate giving rise to a single band at ~3515 cm^{-1}. In the case of Mn2L3_41_AA, there are three red-shifted OH stretches giving rise to two IR bands. The band predicted at ~3520 cm^{-1} is associated with the OH stretching mode involved in the water–perchlorate hydrogen bond, while the second

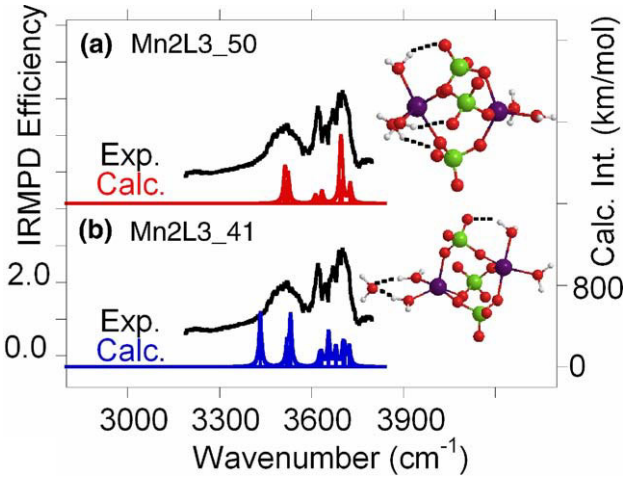

Figure 9. Infrared spectra of $[Mn_2(ClO_4)_3(H_2O)_5]^+$ in the water OH stretching region. In each panel, the experimental spectrum is compared with the calculated IR spectrum for structures Mn2L3_50 (**a**), and Mn2L3_41 (**b**).

one at lower frequency (3433 cm^{-1}) is the signature of the double-acceptor water molecule. The observation of a single IR photodissociation feature below 3600 cm^{-1} for $[Mn_2(ClO_4)_3(H_2O)_5]^+$ may thus suggest that only structures with water–perchlorate hydrogen bonds within the first coordination shell are formed under our experimental conditions. This would also be consistent with the calculated relative energies of the isomers of $[Mn_2(ClO_4)_3(H_2O)_5]^+$ predicting that structures with a double-acceptor water molecule in the second shell are high in energy (Figure 7).

As for $[Mn_2(ClO_4)_3(H_2O)_5]^+$, a red-shifted OH band at ~3520 cm^{-1} characteristic of hydrogen bonded OH is also observed for $[Mn_2(ClO_4)_3(H_2O)_4]^+$. Interestingly, there is a progressive increase of the IR photodissociation signal below 3600 cm^{-1} (Figure 8): whereas no signal is observed in this region for $[Mn_2(ClO_4)_3(H_2O)_2]^+$, a weak and broad signal can be distinguished just below 3600 cm^{-1} for $[Mn_2(ClO_4)_3(H_2O)_3]^+$. These experimental observations are consistent with our theoretical results, which suggest that the lowest-energy structures have all the water molecules in the first coordination shell, and that weak hydrogen bonds are only formed between water and perchlorate. These hydrogen bonds are nearly equivalent and, as can be seen in Figure 8, the corresponding calculated frequency (3510–3530 cm^{-1}) is very close to the position of the band observed experimentally (~3520 cm^{-1}). The progressive increase of the IR photodissociation signal at ~3520 cm^{-1} is also consistent with the fact that the number of water–perchlorate hydrogen bonds increases from zero to three when the lowest-energy structure of the $[Mn_2(ClO_4)_3(H_2O)_5]^+$ (n = 2–5) series is considered (Figure 7).

The detailed assignment of the high-frequency part of the experimental spectra is more difficult and, likely, no single one of the low lying isomers can explain all the observed features. As shown in Figure 8, a relatively sharp band is observed at ~3620 cm^{-1} for all the $[Mn_2(ClO_4)_3(H_2O)_n]^+$ clusters studied here, as well as a broader feature at ~3700 cm^{-1} for n = 3–5. On the basis of the analysis of the normal modes of the lowest lying isomer for each cluster size, one can safely assigned these two bands to the symmetric and asymmetric combinations of the free OH stretches. Interestingly, a common feature is observed at ~3670–3675 cm^{-1} for the three $[Mn_2(ClO_4)_3(H_2O)_n]^+$ (n = 3–5) clusters. These features can be interpreted as an additional evidence for the formation of hydrogen bond since the free OH stretches of the water bound to the perchlorate are predicted ~30 cm^{-1} lower in energy than the ν_{as} OH combination of the free water molecules, as found experimentally.

Overall, the combination of gas-phase infrared spectroscopy and theory provides a consistent picture of the $[Mn_2(ClO_4)_3(H_2O)_n]^+$ clusters studied here. Although the infrared signature of the structures with a double-acceptor water molecule in the second coordination shell might be compatible with the infrared feature

observed at ~3520 cm^{-1}, these structures are much higher in energy than isomers with all the water molecules directly bound to an Mn(II) ion.

Conclusions

Structures of $[Mn(ClO_4)(H_2O)_n]^+$ and $[Mn_2(ClO_4)_3(H_2O)_n]^+$, n = 2–5, were investigated using size selected infrared photodissociation spectroscopy and quantum chemical calculations. For the monometallic species, no spectroscopic evidence of strong water–water hydrogen bonds could be found. These results are consistent with theory, which finds that the lowest energy structures have all the water molecules directly bound to Mn(II). From n = 2 to 4, calculation also suggests that the coordination mode of the perchlorate is η^2, which is confirmed spectroscopically. For $[Mn(ClO_4)(H_2O)_5]^+$, however, theory predicts that the perchlorate has a distorted η^1 coordination, allowing for the direct coordination of five water molecules to the manganese. The resulting lowest energy hexacoordinated Mn(II) complex is also characterized by two water–perchlorate hydrogen bonds. In the case of the bimetallic species, spectroscopic evidence for hydrogen bonding for the largest size clusters were found, in good agreement with the structural and spectral predictions from theory. Spectral assignment of the relatively large $[Mn_2(ClO_4)_3(H_2O)_n]^+$, n = 2–5, complexes could be made assuming that the water molecules bind to an $[Mn_2(ClO_4)_3]^+$ core with the three perchlorate ligands bridging across the two Mn(II) centers. As for the monometallic species, the lowest-energy structures predicted by theory have all the water molecules in the first coordination shell of the metal ions. The red-shifted OH stretching band observed at 3520 cm^{-1} is assigned to an OH stretch associated with a water–perchlorate hydrogen bond, which is predicted to be formed upon the addition of the third water molecule.

Infrared spectroscopy of strongly bound ions with relatively low intensity table top laser in the XH (X = C, N, O) stretching region is challenging. The infrared spectra in the 2600–3800 cm^{-1} spectral range were recorded using a combination of a tunable laser with high power CO_2 laser. Whereas similar combination of infrared lasers has been reported in the past with line tunable CO_2 laser, the herein proposed configuration is simpler to implement and use, and the resulting setup presents an interesting alternative to the tagging technique for spectroscopy of strongly bound ions. The fragmentation yield can be more significantly enhanced by the combination with the CO_2 laser than in the present case when the molecular ion has a good CO_2 chromophore. This is, particularly in the case of phosphorylated peptides, the phosphate group having a large infrared cross section at 10.6 μm. The combination of the CO_2 laser with the infrared free electron laser is also very promising for the investigation of the long wavelength spectral region since the number of IR-FEL photons to be absorbed for inducing the ion fragmentation would otherwise be very large.

Gas-phase ion chemistry has long been a fruitful playground for the interplay between theory and experiment. In the present case, whereas consistent results are obtained using the two approaches, a more extensive exploration of the potential energy surface of both mono- and bimetallic species should be carried out. It should also be noticed that the comparison of experimental and theoretical infrared spectra reveals that the perchlorate Cl–O stretches are unexpectedly underestimated at the B3LYP level of theory. While no definitive conclusions could be drawn concerning the performance of B3LYP for predicting harmonic frequencies, we would like to stress that similar results were obtained for other hypervalent oxides, namely the P–O stretch phosphate groups, during the course of our investigation of both protonated and deprotonated phosphorylated amino-acids and peptides [Sinha, R. K.; Maître, P.; Ohanessian, G., unpublished results].

Acknowledgments

The authors gratefully acknowledge the European Commission for a generous grant (EC15637, 6th FP). They thank the CLIO team (J. M. Ortega, C. Six, G. Perilhous, J. P. Berthet) for their support during the experiments.

Appendix A Supplementary Material

Supplementary material associated with this article may be found in the online version at doi:10.1016/j.jasms.2010.02.014.

References

1. Burgess, J. Metal Ions in Solution; Wiley, London, 1978.
2. Richen, D. T. *The Chemistry of Aqua Ions*; John-Wiley: Chichester; New York, 1997.
3. Kebarle, P. Ion Thermochemistry and Solvation from Gas Phase Ion Equilibria. *Annu. Rev. Phys. Chem.* **1977,** *28*(1), 445–476.
4. Castleman, A. W.; Keesee, R. G. Ionic Clusters. *Chem. Rev.* **1986,** *86*(3), 589–618.
5. Beyer, M. K. Hydrated Metal Ions in the Gas Phase. *Mass Spectrom. Rev.* **2007,** *26*(4), 517–541.
6. Rodgers, M. T.; Armentrout, P. B. Noncovalent Metal-Ligand Bond Energies as Studied by Threshold Collision-Induced Dissociation. *Mass Spectrom. Rev.* **2000,** *19*(4), 215–247.
7. Stace, A. J. Metal ions in Hydrogen Bonded Solvents: A Gas Phase Perspective. *Phys. Chem., Chem. Phys.* **2001,** *3*(11), 1935–1941.
8. Duncan, M. A. Infrared Spectroscopy to Probe Structure and Dynamics in Metal Ion-Molecule Complexes. *Int. Rev. Phys. Chem.* **2003,** *22*(2), 407–435.
9. Walker, N. R.; Walters, R. S.; Duncan, M. A. Frontiers in the Infrared Spectroscopy of Gas Phase Metal Ion Complexes. *New J. Chem.* **2005,** *29*(12), 1495–1503.
10. Lisy, J. M. Spectroscopy and Structure of Solvated Alkali-Metal Ions. *Int. Rev. Phys. Chem.* **1997,** *16*(3), 267–289.
11. Headrick, J. M.; Diken, E. G.; Walters, R. S.; Hammer, N. I.; Christie, R. A.; Cui, J.; Myshakin, E. M.; Duncan, M. A.; Johnson, M. A.; Jordan, K. D. Spectral Signatures of Hydrated Proton Vibrations in Water Clusters. *Science* **2005,** *308*(5729), 1765–1769.
12. Weinheimer, C. J.; Lisy, J. M. Vibrational Predissociation Spectroscopy of $Cs^+H_2O_{1-5}$. *J. Chem. Phys.* **1996,** *105*(7), 2938–2941.
13. Patwari, G. N.; Lisy, J. M. IR Photodissociation Spectroscopy of Na+[H2O](m) [C6F6](n) clusters: Evidence for Separation of Aqueous and Nonaqueous Phases. *J. Phys. Chem. A* **2003,** *107*(45), 9495–9498.
14. Patwari, G. N.; Lisy, J. M. Mimicking the Solvation of Aqueous Na+ in the Gas Phase. *J. Chem. Phys.* **2003,** *118*(19), 8555–8558.

15. Kolaski, M.; Lee, H. M.; Choi, Y. C.; Kim, K. S.; Tarakeshwar, P.; Miller, D. J.; Lisy, J. M. Structures, Energetics, and Spectra of Aqua–Cesium (I) Complexes: An Ab Initio and Experimental Study. *J. Chem. Phys.* **2007,** *126*(7), 074302–074311.
16. Inokuchi, Y.; Ohshimo, K.; Misaizu, F.; Nishi, N. Infrared Photodissociation Spectroscopy of $[Mg.(H_2O)_{1-4}]^+$ and $[Mg.(H_2O)_{1-4}Ar]^+$. *J. Phys. Chem. A* **2004,** *108*(23), 5034–5040.
17. Inokuchi, Y.; Ohshimo, K.; Misaizu, F.; Nishi, N. Structures of $[Mg.(H_2O)_{1,2}]^+$ and $[Al.(H_2O)_{1,2}]^+$ Ions Studied by Infrared Photodissociation spectroscopy: evidence of $[HO\text{-}Al\text{-}H]^+$ ion core structure in $[Al.(H_2O)_2]^+$. *Chem. Phys. Lett.* **2004,** *390*(1–3), 140–144.
18. Bush, M. F.; Saykally, R. J.; Williams, E. R. Infrared Action Spectra of $Ca^{2+}H_2O_{11-69}$ Exhibit Spectral Signatures for Condensed-Phase Structures with Increasing Cluster Size. *J. Am. Chem. Soc.* **2008,** *130*(46), 15482–15489.
19. Bush, M. F.; O'Brien, J. T.; Prell, J. S.; Wu, C. C.; Saylkally, R. J.; Williams, E. R. Hydration of Alkaline Earth Metal Dications: Effects of Metal Ion Size Determined Using Infrared Action Spectroscopy. *J. Am. Chem. Soc.* **2009,** *131*(37), 13270–13277.
20. Rodriguez-Cruz, S. E.; Jockusch, R. A.; Williams, E. R. Hydration Energies and Structures of Alkaline Earth Metal Ions, $M^{2+}(H_2O)_n$, n = 5–7, M = Mg, Ca, Sr, and Ba. *J. Am. Chem. Soc.* **1999,** *121*(38), 8898–8906.
21. Rodriguez-Cruz, S. E.; Jockusch, R. A.; Williams, E. R. Binding Energies of Hexahydrated Alkaline Earth Metal Ions, $M^{2+}(H_2O)_6$, M = Mg, Ca, Sr, Ba: Evidence of Isomeric Structures for Magnesium. *J. Am. Chem. Soc.* **1999,** *121*(9), 1986–1987.
22. Walters, R. S.; Pillai, E. D.; Duncan, M. A. Solvation Dynamics in $Ni^+(H_2O)_n$ Clusters Probed with Infrared Spectroscopy. *J. Am. Chem. Soc.* **2005,** *127*(47), 16599–16610.
23. Carnegie, P. D.; Bandyopadhyay, B.; Duncan, M. A. Infrared Spectroscopy of $Cr^+(H_2O)$ and $Cr^{2+}(H_2O)$: The Role of Charge in Cation Hydration. *J. Phys. Chem. A* **2008,** *112*(28), 6237–6243.
24. Carnegie, P. D.; McCoy, A. B.; Duncan, M. A. IR Spectroscopy and Theory of Cu+(H2O)Ar-2 and Cu+(D2O)Ar-2 in the O–H (O–D) Stretching Region: Fundamentals and Combination Bands. *J. Phys. Chem. A* **2009,** *113*(17), 4849–4854.
25. Walker, N. R.; Walters, R. S.; Pillai, E. D.; Duncan, M. A. Infrared Spectroscopy of $V^+(H_2O)$ and $V^+(D_2O)$ Complexes: Solvent Deformation and an Incipient Reaction. *J. Chem. Phys.* **2003,** *119*(20), 10471–10474.
26. O'Brien, J. T.; Williams, E. R. Hydration of Gaseous Copper Dications Probed by IR Action Spectroscopy. *J. Phys. Chem. A* **2008,** *112*(26), 5893–5901.
27. Sasaki, J.; Ohashi, K.; Inoue, K.; Imamura, T.; Judai, K.; Nishi, N.; Sekiya, H. Infrared photodissociation spectroscopy of $V^+(H_2O)_n$ (n = 2–8): Coordinative saturation of V^+ with four H_2O molecules. *Chem. Phys. Lett.* **2009,** *474*(1–3), 36–40.
28. Iino, T.; Ohashi, K.; Mune, Y.; Inokuchi, Y.; Judai, K.; Nishi, N.; Sekiya, H. Infrared Photodissociation Spectra and Solvation Structures of $Cu^+H_2O_n$ (n = 1–4). *Chem. Phys. Lett.* **2006,** *427*(1–3), 24–28.
29. Iino, T.; Ohashi, K.; Inoue, K.; Judai, K.; Nishi, N.; Sekiya, H. Infrared Spectroscopy of $Cu^+H_2O_n$ and $Ag^+H_2O_n$: Coordination and Solvation of Noble Metal Ions. *J. Chem. Phys.* **2007,** *126*(19), 194302:1–11.
30. Iino, T.; Ohashi, K.; Inoue, K.; Judai, K.; Nishi, N.; Sekiya, H. Coordination and Solvation of Noble Metal Ions: Infrared Spectroscopy of $Ag^+H_2O_n$. *Eur. Phys. J. D: At. Mol. Opt. Plasma Phys.* **2007,** *43*(1), 37–40.
31. Oomens, J.; Sartakov, B. G.; Meijer, G.; Von Helden, G. Gas-Phase Infrared Multiple Photon Dissociation Spectroscopy of Mass-Selected Molecular Ions. *Int. J. Mass Spectrom.* **2006,** *254*(1–2), 1–19.
32. MacAleese, L.; Maître, P. Infrared Spectroscopy of Organometallic Ions in the Gas Phase: From Model to Real World Complexes. *Mass Spectrom. Rev.* **2007,** *26*(4), 583–605.
33. Jaeger, T. D.; van Heijnsbergen, D.; Klippenstein, S. J.; von Helden, G.; Meijer, G.; Duncan, M. A. Vibrational Spectroscopy and Density Functional Theory of Transition-Metal Ion-Benzene and Dibenzene Complexes in the Gas Phase. *J. Am. Chem. Soc.* **2004,** *126*(35), 10981–10991.
34. van Heijnsbergen, D.; von Helden, G.; Meijer, G.; Maître, P.; Duncan, M. A. Infrared Spectra of Gas-Phase V^+(Benzene) and $V^+(Benzene)_2$ Complexes. *J. Am. Chem. Soc.* **2002,** *124*(8), 1562–1563.
35. Polfer, N. C.; Oomens, J.; Moore, D. T.; von Helden, G.; Meijer, G.; Dunbar, R. C. Infrared Spectroscopy of Phenylalanine Ag(I) and Zn(II) Complexes in the Gas Phase. *J. Am. Chem. Soc.* **2006,** *128*(2), 517–525.
36. Polfer, N. C.; Oomens, J.; Dunbar, R. C. IRMPD Spectroscopy of Metal-Ion/Tryptophan Complexes. *Phys. Chem., Chem. Phys.* **2006,** *8*(23), 2744–2751.
37. Dunbar, R. C.; Moore, D. T.; Oomens, J. IR-Spectroscopic Characterization of Acetophenone Complexes with Fe^+, Co^+, and Ni^+ Using Free-Electron-Laser IRMPD. *J. Phys. Chem. A* **2006,** *110*(27), 8316–8326.
38. Moore, D. T.; Oomens, J.; Eyler, J. R.; von Helden, G.; Meijer, G.; Dunbar, R. C. Infrared Spectroscopy of Gas-Phase Cr^+ Coordination Complexes: Determination of Binding Sites and Electronic States. *J. Am. Chem. Soc.* **2005,** *127*(19), 7243–7254.
39. Jagoda-Cwiklik, B.; Jungwirth, P.; Rulisek, L.; Milko, P.; Roithova, J.; Lemaire, J.; Maître, P.; Ortega, J. M.; Schroeder, D. Micro-Hydration of the $MgNO_3^+$ Cation in the Gas Phase. *Chem. Phys. Chem* **2007,** *8*(11), 1629–1639.
40. Mac Aleese, L.; Simon, A.; McMahon, T. B.; Ortega, J. M.; Scuderi, D.; Lemaire, J.; Maître, P. Mid-IR Spectroscopy of Protonated Leucine Methyl Ester Performed with an FTICR or a Paul Type Ion Trap. *Int. J. Mass Spectrom.* **2006,** *249,* 14–20.
41. Bakker, J. M.; Besson, T.; Lemaire, J.; Scuderi, D.; Maître, P. Gas-Phase Structure of a π-Allyl-Palladium Complex: Efficient Infrared Spectroscopy in a 7 T Fourier Transform Mass Spectrometer. *J. Phys. Chem. A* **2007,** *111*(51), 13415–13424.
42. Bakker, J. M.; Sinha, R. K.; Besson, T.; Brugnara, M.; Tosi, P.; Salpin, J. Y.; Maître, P. Tautomerism of Uracil Probed Via Infrared Spectroscopy of Singly Hydrated Protonated Uracil. *J. Phys. Chem. A* **2008,** *112*(48), 12393–12400.
43. Bakker, J. M.; Salpin, J.-Y.; Maître, P. Tautomerism of Cytosine Probed by Gas Phase IR Spectroscopy. *Int. J. Mass Spectrom.* **2009,** *283*(1–3), 214–221.
44. Yeh, L. I.; Okumura, M.; Myers, J. D.; Price, J. M.; Lee, Y. T. Vibrational Spectroscopy of the Hydrated Hydronium Cluster Ions $H_3O^+(H_2O)_n$ (n = 1, 2, 3). *J. Chem. Phys.* **1989,** *91*(12), 7319–7330.
45. Peiris, D. M.; Cheeseman, M. A.; Ramanathan, R.; Eyler, J. R. Infrared Multiple-Photon Dissociation Spectra of Gaseous Ions. *J. Phys. Chem.* **1993,** *97*(30), 7839–7843.
46. Rotzinger, F. P. Performance of Molecular Orbital Methods and Density Functional Theory in the Computation of Geometries and Energies of Metal Aqua Ions. *J. Phys. Chem. B* **2005,** *109*(4), 1510–1527.
47. Duncombe, B. J.; Ryden, J. O. S.; Puskar, L.; Cox, H.; Stace, A. J. A Gas-Phase Study of the Preferential Solvation of Mn^{2+} in Mixed Water/Methanol Clusters. *J. Am. Soc. Mass Spectrom.* **2008,** *19*(4), 520–530.
48. Cox, H.; Akibo-Betts, G.; Wright, R. R.; Walker, N. R.; Curtis, S.; Duncombe, B.; Stace, A. J. Solvent Coordination in Gas-Phase $[Mn(H_2O)_n]^{2+}$ and $[Mn(ROH)_n]^{2+}$ Complexes: Theory and Experiment. *J. Am. Chem. Soc.* **2003,** *125*(1), 233–242.
49. Frisch, M. J.; Trucks, G. W.; Schlegel, H. B.; Scuseria, G. E.; Robb, M. A.; Cheeseman, J. R.; Montgomery, J. A. Jr.; Vreven, T.; Kudin, K. N.; Burant, J. C.; Millam, J. M.; Iyengar, S. S.; Tomasi, J.; Barone, V.; Mennucci, B.; Cossi, M.; Scalmani, G.; Rega, N.; Petersson, G. A.; Nakatsuji, H.; Hada, M.; Ehara, M.; Toyota, K.; Fukuda, R.; Hasegawa, J.; Ishida, M.; Nakajima, T.; Honda, Y.; Kitao, O.; Nakai, H.; Klene, M.; Li, X.; Knox, J. E.; Hratchian, H. P.; Cross, J. B.; Bakken, V.; Adamo, C.; Jaramillo, J.; Gomperts, R.; Stratmann, R. E.; Yazyev, O.; Austin, A. J.; Cammi, R.; Pomelli, C.; Ochterski, J. W.; Ayala, P. Y.; Morokuma, K.; Voth, G. A.; Salvador, P.; Dannenberg, J. J.; Zakrzewski, V. G.; Dapprich, S.; Daniels, A. D.; Strain, M. C.; Farkas, O.; Malick, D. K.; Rabuck, A. D.; Raghavachari, K.; Foresman, J. B.; Ortiz, J. V.; Cui, Q.; Baboul, A. G.; Clifford, S.; Cioslowski, J.; Stefanov, B. B.; Liu, G.; Liashenko, A.; Piskorz, P.; Komaromi, I.; Martin, R. L.; Fox, D. J.; Keith, T.; Al-Laham, M. A.; Peng, C. Y.; Nanayakkara, A.; Challacombe, M.; Gill, P. M. W.; Johnson, B.; Chen, W.; Wong, M. W.; Gonzalez, C.; Pople, J. A. *Gaussian Program Suite*; Gaussian, Inc.: Wallingford, CT, 2004.
50. Herzberg, G. Molecular Spectra and Molecular Structure II. Infrared and Raman Spectra of Polyatomic Molecules, Vol. II; Van Nostrand Reinhold: New York, 1945.
51. Walker, N. R.; Grieves, G. A.; Jaeger, J. B.; Walters, R. S.; Duncan, M. A. Generation of "Unstable" Doubly Charged Metal Ion Complexes in a Laser Vaporization Cluster Source. *Int. J. Mass Spectrom.* **2003,** *228*(2–3), 285–295.
52. Tevault, D. E.; Chi, F. K.; Andrews, L. Infrared Spectrum and Vibrational Potential Function of Chlorite Anion in Matrix-Isolated $M^+ClO_2^-$ species. *J. Mol. Spectrosc.* **1974,** *51*(3), 450–457.